Int. J. Electrochem. Sci., 7 **(2012)** 7993 - 8006

International Journal of
ELECTROCHEMICAL
SCIENCE
www.electrochemsci.org

Influence of Dealloying Solution on the Microstructure of Monolithic Nanoporous Copper through Chemical Dealloying of Al 30 at.% Cu Alloy

Wenbo Liu[1,2,*], *Shichao Zhang*[1,*], *Ning Li*[2], *Jiwei Zheng*[1], *Shenshen An*[1] *and Guangxing Li*[1]

[1] School of Materials Science and Engineering, Beihang University, Beijing 100191, China
[2] School of Manufacturing Science and Engineering, Sichuan University, Chengdu 610065, China
[*]E-mail: liuwenbo_8338@163.com; csc@buaa.edu.cn

Received: 6 July 2012 / *Accepted:* 19 July 2012 / *Published:* 1 September 2012

The monolithic nanoporous copper (NPC) can be achieved through chemical dealloying of melt-spun Al 30 at.% Cu alloy comprising α-Al and Al_2Cu in a hydrochloric acid (HCl) or sodium hydroxide (NaOH) aqueous solution under free corrosion conditions, during which influence of dealloying solution on the microstructure was investigated, and their formation mechanism is discussed. The microstructure of the NPC ribbons was characterized using X-ray diffraction, scanning electron microscopy, energy dispersive X-ray analysis, transmission electron microscopy, and high-resolution transmission electron microscopy. The experimental results show that the Al 30 at.% Cu alloy presents markedly different microstructure characteristics upon the dealloying in the acidic/alkaline corrosive environment, indicating dealloying solution has a significant influence on the dealloying process and the microstructure of NPC. This is closely related to the difference between electrochemical activities of α-Al and Al_2Cu in the initial alloy in the distinct corrosion media. Additionally, the length scales of ligaments/channels in the NPC can be tuned via simply changing the dealloying solution, which results from the different surface diffusivity of Cu atoms along the alloy/solution interfaces in the acidic/alkaline solution. According to the ligament sizes, the surface diffusivity of Cu atoms in the HCl solution can be evaluated as 1.79×10^{-16} m^2 s^{-1}, which is approximately two orders of magnitude greater than that in the NaOH solution (3.15×10^{-19} m^2 s^{-1}).

Keywords: Nanoporous copper; Dealloying; Corrosion media; Microstructure; Surface diffusivity

1. INTRODUCTION

Nanoporous metals (NPMs), as novel functional materials, have recently attracted considerable interest in a wide variety of applications including catalysis, sensors, actuators, fuel cells, microfluidic flow controllers, and so forth [1-4]. For a long time past, template methods are commonly used to

fabricate these materials through the replication of porous alumina or liquid-crystal templates [5-7]. Since it has been found that chemical/electrochemical dealloying can be used to yield a broad range of porous metals, during the latest decades, a great deal of effort has been directed towards the investigation of NPMs through dealloying [8-11]. However, most of the previously reported porous metals were fabricated by dealloying from binary/ternary alloy systems with a single-phase solid solubility across all compositions, which refer to selective dissolution of one or more active components out of an alloy, such as Cu-Pt, Ag-Au, Cu-Au, and Au-Ag-Pt [12-15]. In view of their industrial applications, widespread uses of the dealloying technique to make NPMs are frequently hindered by the high cost of these noble metals and the limited alloy systems. Thus, fabrication of NPMs from alloy families based on common metals with multiple phases needs to be investigated.

Lu et al. [16] reported that porous copper, which had a significantly large channel size (~ 500 nm), can be synthesized from nanocrystalline two-phase Cu-Zr films by electrochemical dealloying in an acidic solution, but no obvious porous structure can be obtained from the as-cast Cu–Zr alloys under the same conditions. Zhang et al. [17] fabricated monolithic NPC with a ligament/channel size of several hundreds of nm from dual-phase Al-Cu alloys by chemical dealloying in a HCl solution. Recently, our group also synthesized several kinds of NPC with complicated ligament-channel structures from multi-phase M-Cu alloy systems through facile chemical dealloying in some specific corrosion media [18-20]. Unfortunately, studies on influence of dealloying solution on the microstructure of these NPC could not be systematically conducted until now, while it would be conducive to understanding underlying physical mechanism of dealloying of multi-phase alloys and opening a window towards achieving the attempts to fabricate novel NPMs from broad alloy families with multiple phases.

It has been recognized that the electrochemical activity of some phase in a multi-phase alloy system is significantly different relative to a different corrosive environment, thus strongly affecting the dissolution process and microstructure of resulting products. From this perspective, we herein employ HCl and NaOH solutions as typical dealloying media to principally investigate the influence of dealloying solution on the microstructure of monolithic NPC from Al 30 at.% Cu alloy. The results show that the Al-Cu alloy presents remarkably different microstructure characteristics (including surface morphology and ligament/channel sizes) upon the dealloying in the acidic/alkaline corrosive environment, indicating dealloying solution has a significant influence on the dealloying process and microstructure of NPC. Based on our current understanding of dealloying process, their formation mechanism has been discussed in detail. Additionally, the length scales of ligaments/channels in the NPC can be tuned via simply changing the dealloying solution.

2. EXPERIMENTAL SECTION

Al-Cu alloy with nominal composition of 30 at.% Cu was prepared from pure Al (99.99 wt.%) and pure Cu (99.999 wt.%). Voltaic arc heating was employed to melt the charges in a copper crucible under an argon atmosphere, and then the melt was cooled down into ingots in situ. By use of a single roller melt spinning apparatus, the Al-Cu ingots were remelted in a quartz tube by high-frequency

induction heating and then melt-spun onto a copper roller at a circumferential speed of ~3000 rpm in a controlled argon atmosphere. The alloy ribbons obtained were typically 20-40 μm in thickness, 4-6 mm in width, and several centimeters in length. The dealloying of the melt-spun Al-Cu ribbons was performed in 5 wt.% HCl aqueous solution at 75 °C and 10 wt.% NaOH aqueous solution at room temperature (RT) for different times, respectively. After dealloying, the samples were rinsed with distilled water and dehydrated alcohol. The as-dealloyed samples were kept in a vacuum chamber to avoid oxidation. Microstructural characterization and analysis of the melt-spun Al 30 at.% Cu alloy ribbons and as-dealloyed samples were made using X-ray diffraction (XRD, Rigaku D/Max-2400) with Cu Kα radiation, scanning electron microscopy (FESEM, Hitachi S-4800) with an energy dispersive X-ray analyzer (EDX), transmission electron microscopy (TEM, JEOL JEM 2100F) with selected-area electron diffraction (SAED), and high-resolution transmission electron microscopy (HRTEM, JEOL JEM 2100F). To test the electrochemical activities of α-Al and Al_2Cu phases in the melt-spun Al 30 at.% Cu alloy, potentiodynamic polarizations studies were conducted on single-phase α-Al solid solution and Al_2Cu intermetallics (corresponding to Al-Cu alloy with a trace amount of Cu and Al 33 at.% Cu alloy) in the 5 wt.% HCl solution at 75 °C and 10 wt.% NaOH solution at RT by using an electrochemical measurement unit (PARSTAT 2273), respectively. The experiments were carried out in a standard three-electrode electrochemical cell (200mL) with a Pt plate electrode as a counter electrode, a saturated calomel electrode (SCE) as a reference electrode, and the alloy ribbon as the working electrode. Polarization scan was performed towards positive values at a scan rate of 1.0 mV s^{-1}, after allowing a steady state potential to develop. In order to evaluate specific surface areas of the as-obtained porous products, the N_2 adsorption/desorption experiments were carried out at 77 K on a Nova Station A automatic surface area and pore radius distribution apparatus.

3. RESULTS AND DISCUSSION

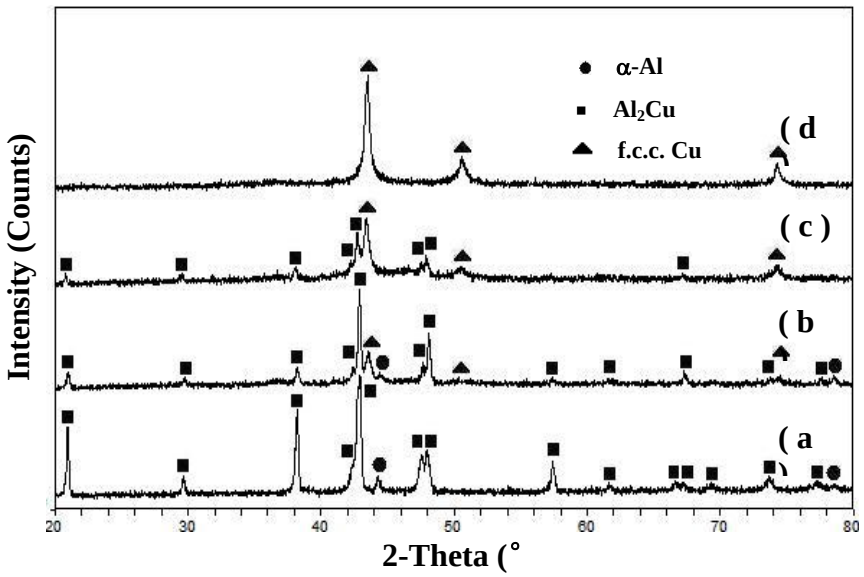

Figure 1. XRD patterns of melt-spun Al 30 at.% Cu alloy ribbons (a) before and (b-d) upon dealloying in the 5 wt.% HCl solution at 75 °C for 4 min, 10 min, 30 min.

Figure 1 shows the XRD patterns of the starting melt-spun Al 30 at.% Cu alloy and the as-dealloyed samples upon dealloying in the HCl solution for different times, respectively. The filled circles, squares and triangles in Figure 1 stand for α-Al, Al_2Cu and Cu, respectively. The Al 30 at.% Cu alloy is composed of two distinct phases: α-Al and Al_2Cu (Figure 1a), while the Al_2Cu phase is markedly dominant in the alloy. As can be seen from Figure 1b-d, with the increase of dealloying times, the peak intensities of α-Al and Al_2Cu phases decrease nearly simultaneously where that of Al_2Cu phase decrease faster than α-Al, and in the meantime, counterparts of Cu phase emerge and continually increase. Finally, only a face-centered cubic (f.c.c.) Cu phase can be identified in the as-dealloyed samples upon the dealloying for 30 min. It indicates clearly that α-Al and Al_2Cu phases in the alloy can be almost simultaneously dealloyed in the HCl solution, but just Al_2Cu phase is dissolved faster.

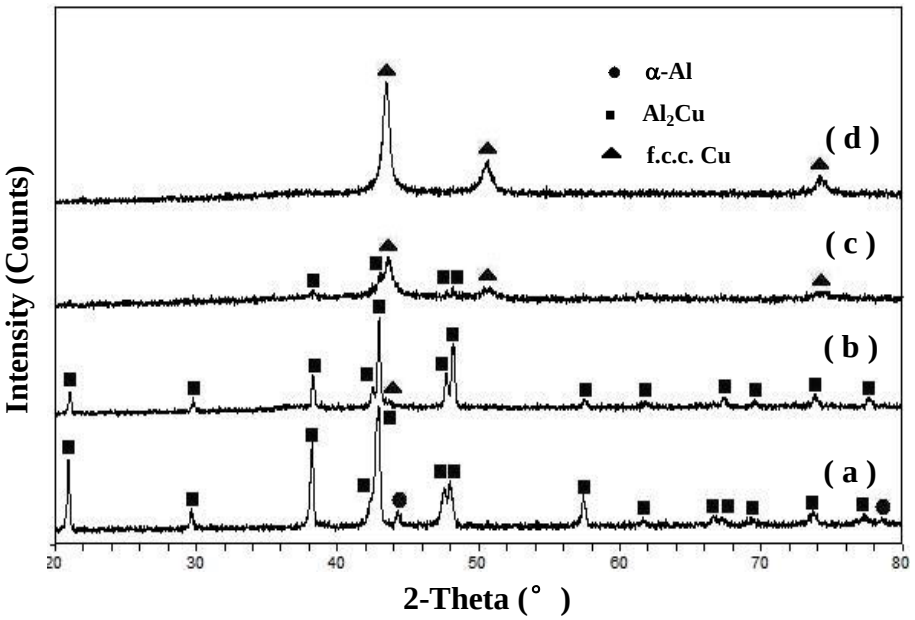

Figure 2. XRD patterns of melt-spun Al 30 at.% Cu alloy ribbons (a) before and (b-d) upon dealloying in the 10 wt.% NaOH solution at RT for 0.5 h, 1 h, 3 h.

Figure 2 shows the XRD patterns of the as-dealloyed samples upon dealloying in the NaOH solution for different times, respectively. For clear comparison, the XRD pattern of the initial alloy is also added in Figure 2. It can be seen that the peak intensities of all the α-Al phase disappear quickly while counterparts of Al_2Cu phase have little change in the as-dealloyed samples upon the dealloying for 0.5 h, and note that, at this moment, no obvious Cu phase can be detected. With the further increase of dealloying times, the peak intensities of Al_2Cu phase decrease slowly and gradually disappear, and only a single f.c.c. Cu phase can be detected until the dealloying time up to 3 h. It suggests that α-Al phase can be selectively preferentially dissolved in the NaOH corrosive environment prior to the etching of Al_2Cu phase.

Figure 3 shows the microstructure of the as-dealloyed samples upon dealloying in the HCl solution for different times, respectively. For the as-dealloyed samples for 4 min, a nearly uniform

ligament-channel structure can be observed in the grains while just a slight etching occurs in the region of grain boundary (GB), as marked by upward and downward arrows in Figure 3b, respectively.

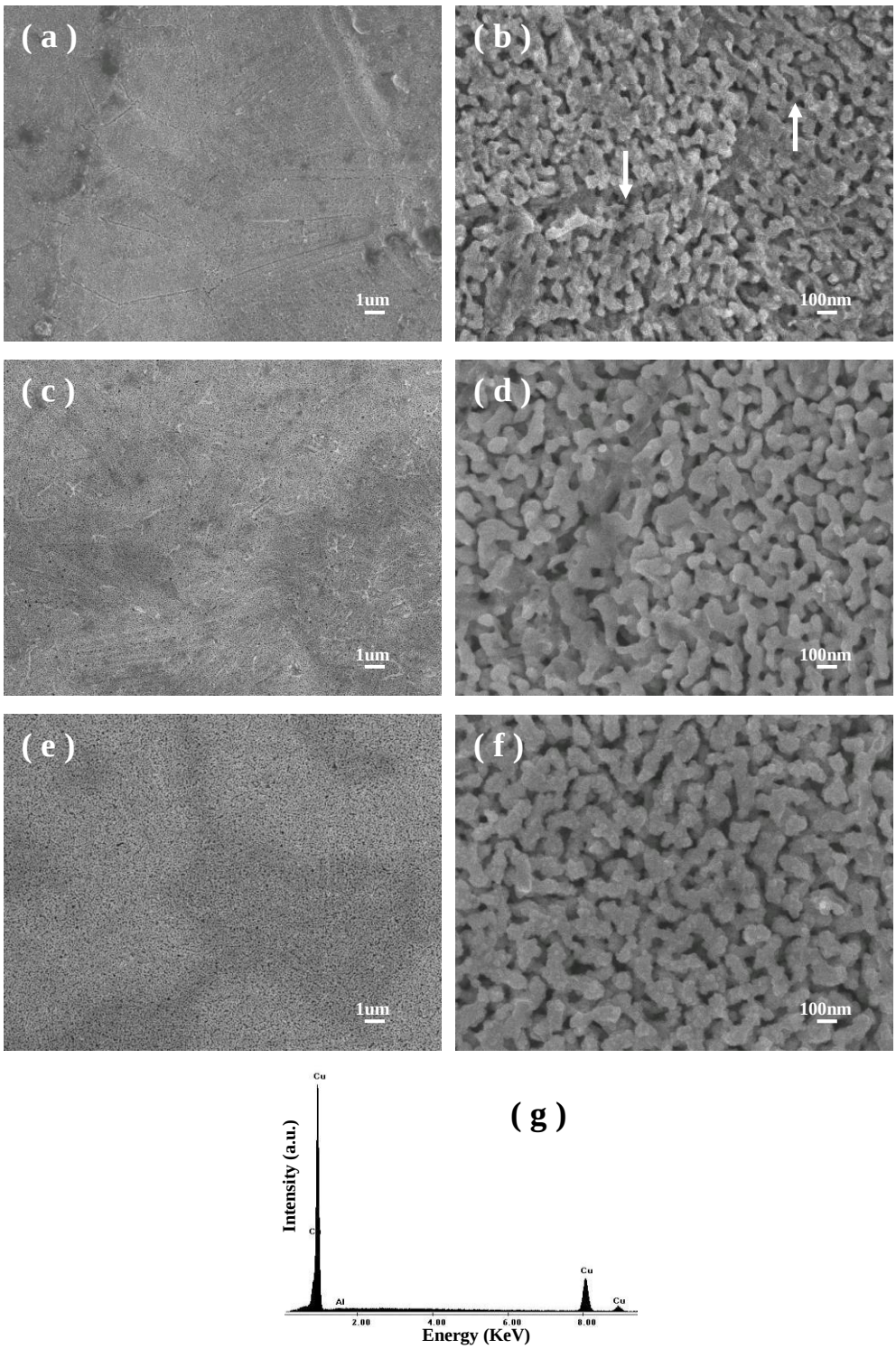

Figure 3. SEM images showing the microstructure of as-dealloyed samples by dealloying in the 5 wt.% HCl solution at 75°C for (a-b) 4 min, (c-d) 10 min, (e-f) 30 min. Parts b, d and f show the microstructures at a higher magnification. (g) EDX spectrum of NPC upon dealloying in the HCl solution for 30 min. a.u.: arbitrary units.

With the dealloying time up to 30 min, the region of GB can be gradually dealloyed, eventually resulting in the formation of NPC with a uniform ligament-channel structure with length scales of ~90±10 nm. EDX analysis has been performed on the NPC ribbons by dealloying in the HCl solution for 30 min, and the corresponding spectrum is shown in Figure 3g. It is obvious that nearly all of Al is removed from the Al 30 at.% Cu alloy during dealloying in the HCl solution.

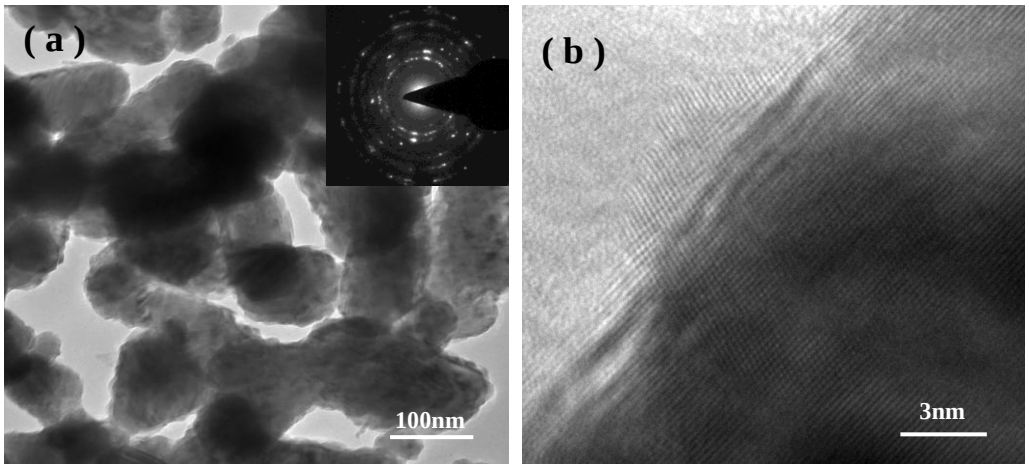

Figure 4. (a) TEM image showing the porous structure of the NPC ribbons by dealloying of the Al 30 at.% Cu alloy in the 5 wt.% HCl solution at 75°C for 30 min. (Inset) SAED pattern corresponding to one ligament in part a. (b) HRTEM image shows the crossed lattice fringes in the ligament of NPC.

TEM observation further verifies the uniform porous structure of the NPC upon dealloying in the HCl solution for 30 min and one typical TEM bright-field image is shown in Figure 4a. It is clear that the ligament edges are coarse and accumulated by fine particles. The SAED pattern mainly consists of polycrystalline rings, corresponding to f.c.c. $(111)_{Cu}$, $(200)_{Cu}$, $(220)_{Cu}$, and $(311)_{Cu}$ reflections (inset of Figure 4a). Moreover, the crossed lattice fringes in the ligament from the HRTEM image (Figure 4b) further demonstrate that the ligaments in the NPC comprise Cu polycrystals rather than the monocrystals typically obtained in the ligaments of NPG through dealloying of the prototypical Ag-Au system [21], which is probably related to the secondary nucleation or recrystallization driven by high temperature [22-26].

Figure 5 shows the SEM images of the as-dealloyed samples upon dealloying in the NaOH solution for different times, respectively. It is obvious that the region of GB can be preferentially dissolved to form the large-sized channels with length scales of hundreds of nm in the as-dealloyed samples upon the dealloying for 0.5 h; it should be noted that, however, these large-sized channels are not cracks. In contrast, no obvious etching phenomena can be observed in the grains at this dealloying stage. With the dealloying time up to 3 h, the dealloying in the grains gradually takes place, leading to the formation of NPC with an open, bicontinuous interpenetrating ligament-channel structure with length scales of 30±10 nm in the grains. Obviously, the resultant NPC ribbons have bimodal channel

size distributions composed of large-sized channels (hundreds of nm) with highly porous channel walls (tens of nm). Both large- and small-sized channels are 3D, open and bicontinuous.

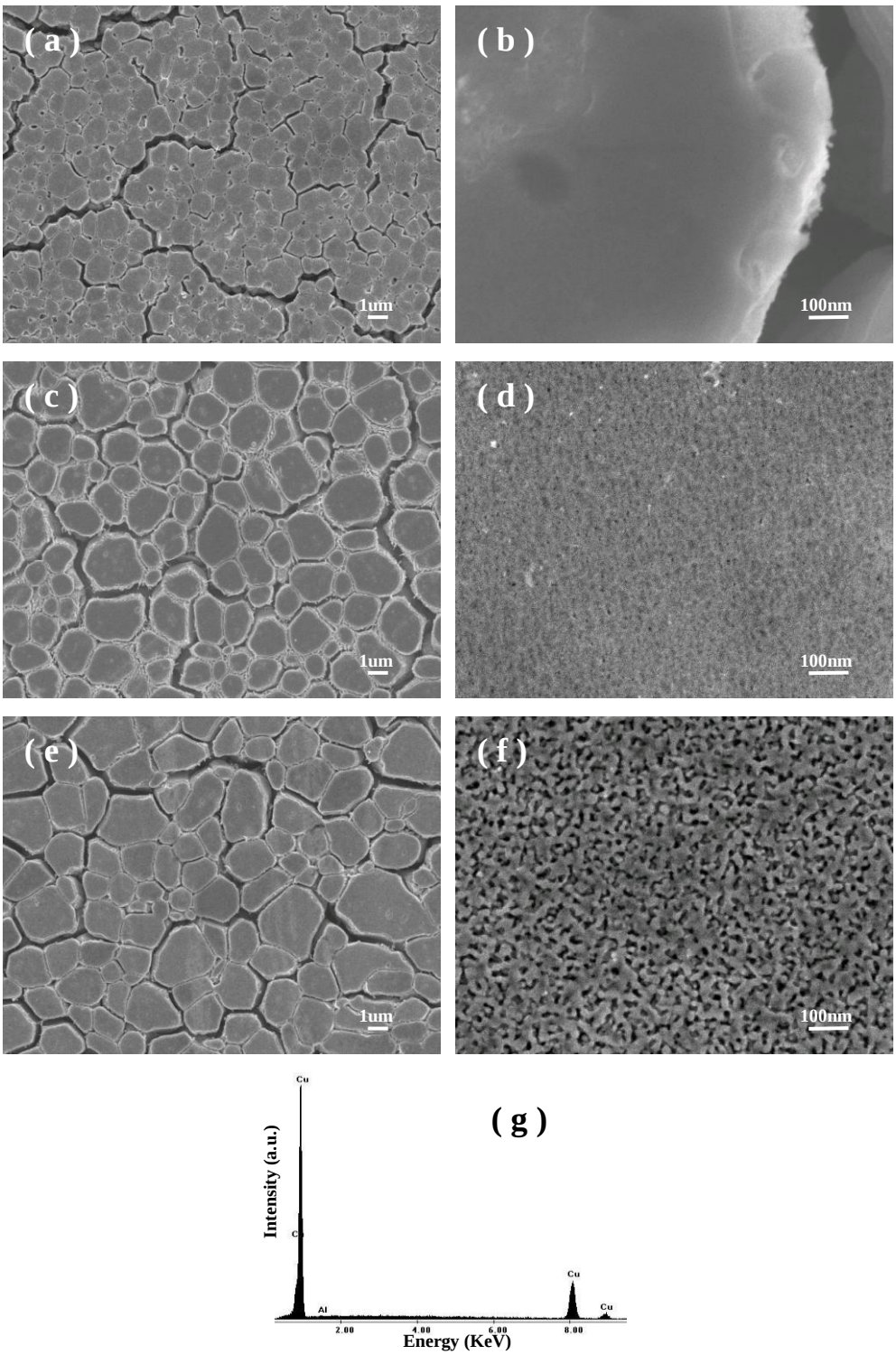

Figure 5. SEM images showing the microstructure of NPC by dealloying in the 10 wt.% NaOH solution at RT for (a-b) 0.5 h, (c-d) 1 h, (e-f) 3 h. Parts b, d and f show the microstructures at a higher magnification. (g) EDX spectrum of NPC upon dealloying in the NaOH solution for 3 h. a.u.: arbitrary units.

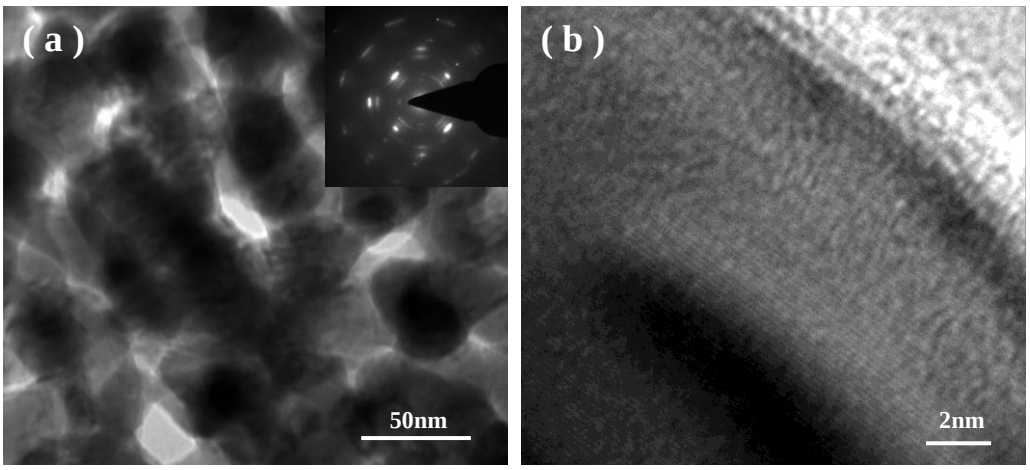

Figure 6. (a) TEM image showing the porous structure of the NPC ribbons by dealloying of the Al 30 at.% Cu alloy in the 10 wt.% NaOH solution at RT for 3 h. (Inset) SAED pattern corresponding to one ligament in part a. (b) HRTEM image shows lattice fringes extending throughout the whole ligament.

Intriguingly, the walls of these large-sized channels form island-shaped structures and it is reasonable to assume that the morphology and sizes of these island-shaped structures in the NPC inherit from the Al_2Cu grains in the initial Al-Cu alloy on a basis of a combination of XRD analysis and SEM observations. Additionally, EDX analysis in Figure 5g shows only Cu can be identified and nearly all of Al was etched away during dealloying by the NaOH solution.

Figure 6 shows the typical TEM images of porous structure of the NPC ribbons upon dealloying in the NaOH solution for 3 h. It is obvious that the smooth ligament edges can be observed in the as-dealloyed samples. A SAED pattern corresponding to one ligament shows a hexagonal pattern, which is from the f.c.c. Cu [110] zone axis, indicating a single crystalline characteristic of the selected area (inset of Figure 6a). Moreover, lattice fringes extending throughout the whole ligament from the HRTEM image in Figure 6b further verify the single crystal nature of the ligament in the NPC. It should be noted that, however, the present results are essentially different from the established notion that the crystal lattice orientation is retained during dealloying of Ag-Au alloys with the conservation of the grain size of the master alloys [21,27-29]. For the lattice structure of the resulting NPC is considerably different from that of Al_2Cu intermetallics in the initial Al-Cu alloy (Al_2Cu: body centered tetragonal; Cu: f.c.c.).

It should be noted that the length scales of ligaments/channels in the NPC upon dealloying in the NaOH solution are significantly small compared to those in the HCl solution, which can be confirmed by XRD results because of the remarkable increase of peak width of reflections more sensitive to the change in structure size of Cu phase. Additionally, we note that the color of the NPC ribbons upon dealloying in the HCl solution is very close to that of bulk solid copper (Figure 7b), indicating the coarse porous structure in the NPC. In contrast, the color of the copper surface upon dealloying in the NaOH solution becomes dark (Figure 7a) due to its high surface area and nano-sized structure [30].

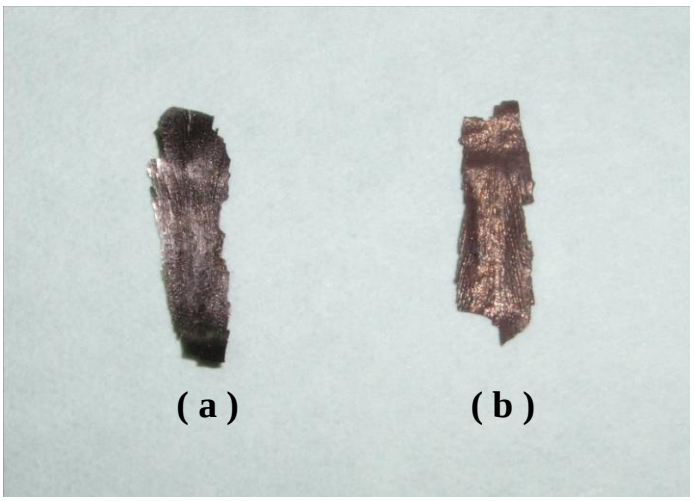

Figure 7. Macrographs of the as-dealloyed samples upon chemical dealloying (a) in the NaOH solution, (b) in the HCl solution.

Table 1. Chemical composition of typical island-shaped structure by EDX analysis in the as-dealloyed samples upon dealloying in the NaOH solution for 0.5 h.

Structure	Elements (at.%)	
	Al	Cu
Island-shaped	65.24	34.76

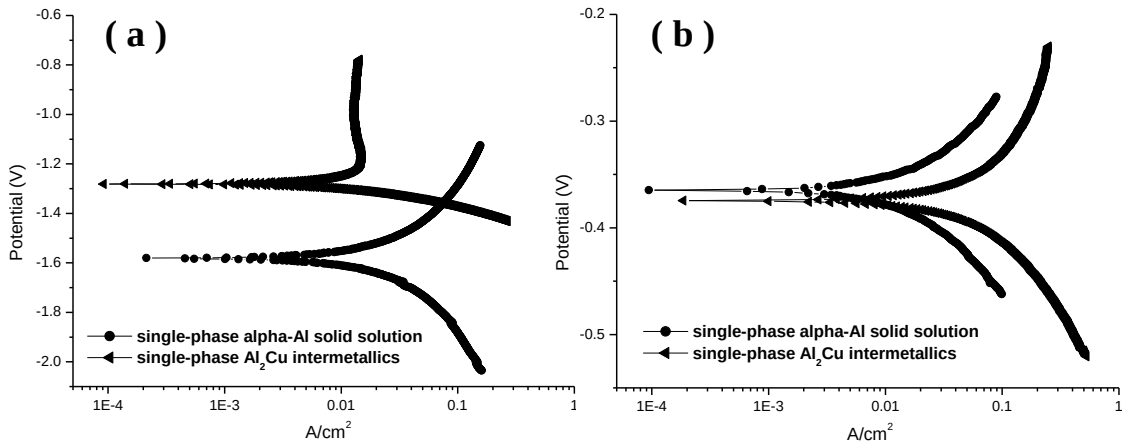

Figure 8. Tafel polarization curves of single-phase α-Al solid solution and Al_2Cu intermetallics (a) in the NaOH solution, (b) in the HCl solution.

Table 1 shows the chemical composition of typical island-shaped structure by EDX analysis in the as-dealloyed samples upon dealloying in the NaOH solution for 0.5 h. The results show that the island-shaped structure is enriched in Al, and the atomic percentage of Al to Cu in the island-shaped structure is close to 2:1. Combined with the XRD results in Figure 2, it can be confirmed that the island-shaped structure is Al_2Cu phase.

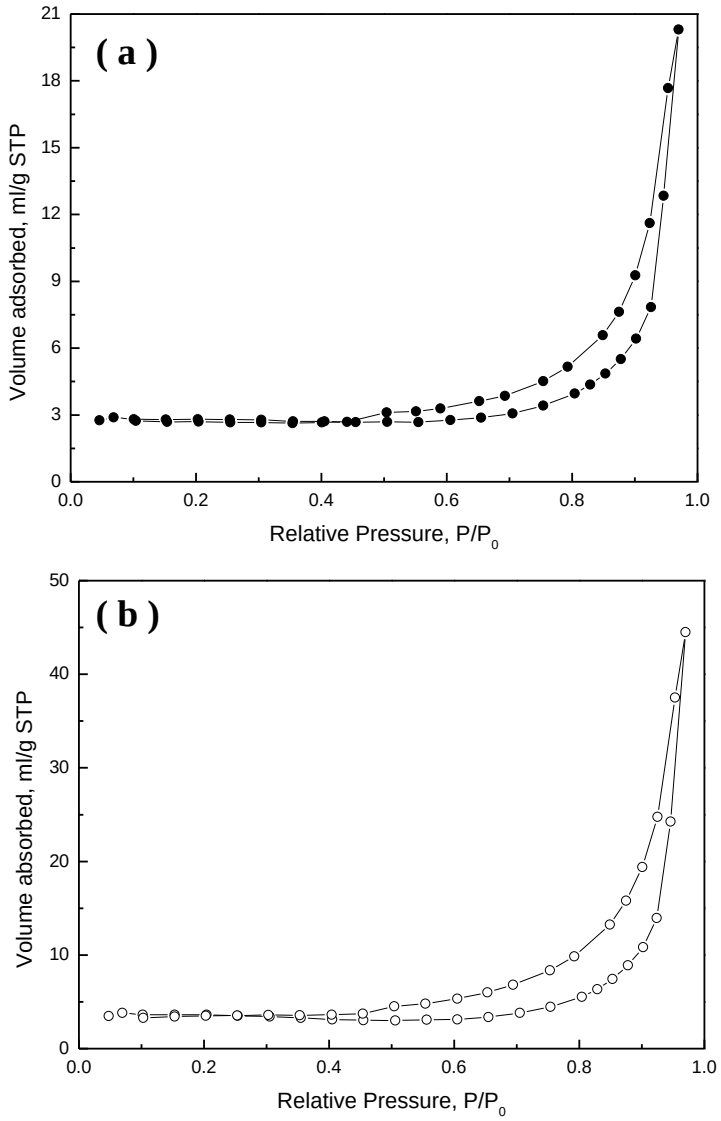

Figure 9. N_2 isotherms at 77 K for the NPC ribbons by dealloying of the Al 30 at.% Cu alloy (a) in the HCl solution at 75°C for 30 min, (b) in the NaOH solution at RT for 3 h.

Figure 8 shows Tafel polarization curves of single-phase α-Al solid solution and Al_2Cu intermetallics in the HCl and NaOH solutions, respectively. It can be found that in the NaOH solution, the difference between corrosion potentials of single-phase α-Al solid solution and Al_2Cu intermetallics is ~299 mV(SCE), much greater than that in the HCl solution (~9.91 mV(SCE)). The present results clearly indicate that α-Al and Al_2Cu have the close electrochemical activities in the acidic solution, while a relatively high electrochemical activity can be obtained for α-Al in the alkaline solution compared to Al_2Cu.

The specific surface areas of these resultant porous products can be evaluated based upon N_2 adsorption/desorption experiments. Figure 9 shows the N_2 adsorption/desorption isotherms for the NPC ribbons by dealloying of the melt-spun Al 30 at.% Cu alloy in the 5 wt.% HCl/10 wt.% NaOH solution. The result shows that the Brunauer-Emmett-Teller (BET) surface areas of the appointed porous products by dealloying in the HCl and NaOH solutions are much high and have been

determined to be 11.6±0.1 and 18.7±0.1 $m^2 g^{-1}$, respectively. It is worthwhile noting that the interesting structural feature upon dealloying in the NaOH solution endows the NPC with higher surface area, which is especially beneficial for catalysis and sensing applications.

It is generally recognized that ideal bicontinuous nanoporous structures are obtained from binary alloy families with a single-phase solid solubility across all compositions by chemical/electrochemical dealloying. The formation mechanism of nanoporous structures during dealloying has been described in the literature [8]. It has been shown that ligaments form as a result of an intrinsic pattern formation during which aggregation of chemically driven noble metal atoms occurs. The process started with selective dissolution of base metal atoms from the outermost alloy surface, leaving behind noble metal atoms that diffused along alloy/solution interfaces and agglomerated into the ligaments. Thus, porosity evolution forms dynamically during dissolution and is not due to one active component simply being excavated out of a binary alloy [31].

However, if multiple phases exist in an alloy, a more complicated process would occur during dealloying. In this case, the present Al 30 at.% Cu alloy is composed of α-Al and Al_2Cu phases. According to the non-equilibrium solidification theory, during the rapid solidification of Al 30 at.% Cu alloy, primary Al_2Cu phases precipitate firstly and α-Al solid solution subsequently forms from the remaining liquid, suppressing the occurrence of eutectic reaction due to the fast cooling rate, characteristic of α-Al phase surrounding primary Al_2Cu phase (namely, divorced eutectic structure).

As indicated in Figure 8, the disparity between electrochemical activities of α-Al and Al_2Cu phases in the initial alloy is very small in the HCl solution, while relatively large one is achieved in the NaOH solution. Thus, α-Al and Al_2Cu phases can be almost simultaneously dissolved in the acidic solution, where Al_2Cu in the grains can be relatively dissolved faster due to its slightly higher electrochemical activity. For this reason, a nearly uniform ligament-channel structure can be preferentially formed in the grains while a relatively slight etching process occurs in the region of GB (corresponding to the dissolution of α-Al) in the as-dealloyed samples upon the dealloying just for 4 min. Subsequently, as a result of the synergetic dealloying of the coexisting α-Al and Al_2Cu phases in the Al-Cu alloy, the NPC with a homogenous ligament-channel structure can be fabricated by dealloying in the HCl solution for 30 min.

Contrarily, in the alkaline corrosive environment, the electrochemical activity of α-Al phase is much higher than Al_2Cu. α-Al and Al_2Cu phases existing in the alloy can form corrosion couple cells due to the large difference between electrochemical activities of two distinct phases, with the α-Al phase acting as an anode and preferentially dissolving compared with the Al_2Cu. Thus, the dealloying of the dual-phase alloy in the NaOH solution will take place in a specific sequence, namely first confined to the α-Al phase in the region of GB, and then spreading out in the Al_2Cu phase in the grains. The excavation of α-Al phase from the dual-phase alloy contributes to the formation of the large-sized channels in the resultant NPC, while the dealloying of the Al_2Cu phase results in the nanoporous structure of the channel walls. Obviously, it is in good agreement with the SEM observations. This is why the NPC with bimodal channel size distributions can be obtained upon dealloying in the NaOH solution for 3 h. Therefore, the same Al-Cu alloy takes on the different dealloying morphologies during/upon dealloying in the acidic/alkaline corrosion medium and we can

conclude that dealloying solution has a key influence on the dealloying process and the microstructure of NPC.

It is known that the evolution of porous structure during dealloying involves etching of less noble (LN) element coupled with coarsening of more noble (MN) element by surface diffusion. Surface diffusion of MN element along alloy/solution interfaces plays a key role in the formation of NPMs and has a significant influence on the length scales of ligaments/channels [8,31]. It has been found that during the dealloying of Al-based alloys in alkali solution, as a result of the formation of MN-hydroxy species, the interaction of MN atoms and OH^-, and the low solubility of AlO_2^-, surface diffusivity of the MN atoms is significantly reduced compared to that in acid media [32-35]. These will be further discussed based on the calculations on the surface diffusivity in the following section.

It has been reported that a maximally unstable spatial period relationship has been predicted for the characteristic length scale (d) of NPMs and surface diffusivity (D_S): $d \propto (D_S / V_0)^{\mu}$, where V_0 is the velocity of a flat alloy surface with no MN atoms accumulated upon it and μ is a constant, suggested to be 1/6 or 1/4 [8,36]. Based on the surface diffusion controlled coarsening mechanism, the D_S values of Cu atoms along alloy/solution interfaces can be estimated by the equation [36-37]:

$D_S = \frac{[d(t)]^4 kT}{32\gamma t\alpha^4}$ (1), where k is the Boltzmann constant (1.3806×10^{-23} J K^{-1}), γ is the surface energy (1.79 J m^{-2}) [38], $d(t)$ is the ligament size at the dealloying time t, α is the lattice parameter of Cu (3.6153×10^{-10} m), and T is the dealloying temperature. According to the ligament sizes in the NPC ribbons, the D_S of Cu atoms along alloy/solution interfaces was calculated for dealloying of Al 30 at.% Cu alloy in the HCl/NaOH solution, as listed in Table 2.

Table 2. The ligament sizes in NPC ribbons by dealloying of Al 30 at.% Cu alloy in the HCl/NaOH solution, the corresponding surface diffusivities estimated by Eq. (1) [36-37].

Dealloying solution	HCl	NaOH
Dealloying temperature (T, K)	348	298
Dealloying time (t, s)	1800	10800
Ligament sizes (d(t), nm)	90±10	30±10
Surface diffusivity (D_S, m^2 s^{-1})	1.79×10^{-16}	3.15×10^{-19}

It is astonishing that the D_S of Cu atoms in the acidic solution, 1.79×10^{-16} m^2 s^{-1}, is approximately two orders of magnitude greater than that in the alkaline solution (3.15×10^{-19} m^2 s^{-1}), indicating the occurrence of substantial structure coarsening with greater diffusivity in the acidic solution. This is why an evidently small ligament-channel structure can be obtained in the as-dealloyed samples upon dealloying in the NaOH solution compared with relatively large one formed in the HCl solution.

Most previous attention is mainly focused on the dealloying of single-phase alloy systems with a solid solubility across all compositions (Ag-Au, Mn-Cu, etc.) [8,31]. Obviously, the dealloying of multi-phase alloy systems will be more complicated due to the great difference in lattice structures.

Based on the present work, we are confident that it will have important implications for understanding the underlying physical mechanism of dealloying of multi-phase alloys, fabricating and tailoring the porous materials with different ligament-channel structures via controlling the dissolution processes among different phases, and thus further exploring their promising applications in broader fields, such as lithium ion batteries. Some encouraging test findings have been obtained in our previous work [39-41], the extensive study is in progress.

4. CONCLUSION

In summary, monolithic NPC ribbons can be fabricated through chemical dealloying of melt-spun Al 30 at.% Cu alloy comprising α-Al and Al_2Cu in an acidic or alkaline solution under free corrosion conditions. The dealloying solution has a significant influence on the dealloying process and the microstructure of NPC. In an acidic corrosive environment, α-Al and Al_2Cu phases in the initial alloy can be almost simultaneously dissolved to form the NPC with a homogenous ligament-channel structure, while the dealloying of the dual-phase alloy in the alkaline solution will take place in a specific sequence, eventually resulting in the formation of NPC with bimodal channel size distributions. It can be attributed to the disparity between electrochemical activities of α-Al and Al_2Cu phases in the initial alloy in the different corrosion media. Additionally, an evidently small ligament/channel sizes can be obtained in the as-dealloyed samples upon dealloying in the NaOH solution compared to relatively large one formed in the HCl solution, which mainly derives from the lower surface diffusivity of Cu atoms along the alloy/solution interfaces in the alkaline solution.

ACKNOWLEDGEMENT
We give thanks to financial support by the State Key Basic Research Program of PRC (2007CB936502), the National Natural Science Foundation of China (50574008, 50954005, 51074011), the National 863 Program Project (2006AA03Z230, 2008AA03Z208), the China Postdoctoral Science Foundation Funded Project (2011M500214), and the Basic Research Fund Project of Beihang University (501LJJC2012101001). Also, we are grateful to Prof. T. Zhang and Dr. J.F. Wang for assistance in preparation of the starting alloy ribbons.

References

1. G. C. Bond and D. T. Thompson, *Catal. Rev.*, 41 (1999) 319.
2. T. You, O. Niwa, M. Tomita and S. Hirono, *Anal. Chem.*, 75 (2003) 2080.
3. J. R. Weissmueller, N. Viswanath, D. Kramer, P. Zimmer, R. Wuerschum and H. Gleiter, *Science*, 300 (2003) 312.
4. S. H. Joo, S. J. Choi, K. J. Kwa and Z. Liu, *Nature*, 412 (2001) 169.
5. H. Masuda and K. Fukuda, *Science*, 268 (1995) 1466.
6. G. S. Attard, P. N. Bartlett, N. R. B. Coleman, J. M. Elliott, J. R. Owen and J. H. Wang, *Science*, 278 (1997) 838.
7. T. Kijima, T. Yoshimura, M. Uota, T. Ikeda, D. Fujikawa, S. Mouri and S. Uoyama, *Angew. Chem., Int. Ed.*, 43 (2004) 228.

8. J. Erlebacher, M. J. Aziz, A. Karma, N. Dimitrov and K. Sieradzki, *Nature*, 410 (2001) 450.
9. C. X. Ji and P. C. Searson, *J. Phys. Chem. B*, 107 (2003) 4494.
10. M. Stratmann and M. Rohwerder, *Nature*, 410 (2001) 420.
11. W. B. Liu, S. C. Zhang, N. Li, J. W. Zheng and Y. L. Xing, *Int. J. Electrochem. Sci.*, 6 (2011) 5445.
12. D. V. Pugh, A. Dursun and S. G. Corcoran, *J. Electrochem. Soc.*, 152 (2005) B455.
13. U. S. Min and J. C. M. Li, *J. Mater. Res.*, 9 (1994) 2878.
14. B. W. Parks Jr., J. D. Fritz and H. W. Pickering, *Scripta Mater.*, 23 (1989) 951.
15. J. Snyder, P. Asanithi, A. B. Dalton and J. Erlebacher, *Adv. Mater.*, 20 (2008) 4883.
16. H. B. Lu, Y. Li and F. H. Wang, *Scripta Mater.*, 56 (2007) 165.
17. Z. Qi, C. C. Zhao, X. G. Wang, J. K. Lin, W. Shao, Z. H. Zhang and X. F. Bian, *J. Phys. Chem. C*, 113 (2009) 6694.
18. W. B. Liu, S. C. Zhang, N. Li, J. W. Zheng, S. S. An and Y. L. Xing, *Int. J. Electrochem. Sci.*, 7 (2012) 6365.
19. W. B. Liu, S. C. Zhang, N. Li, J. W. Zheng and Y. L. Xing, *Microporous Mesoporous Mater.*, 138 (2011) 1.
20. W. B. Liu, S. C. Zhang, N. Li, J. W. Zheng, S. S. An and Y. L. Xing, *Int. J. Electrochem. Sci.*, 7 (2012) 2240.
21. Y. Ding, Y. J. Kim and J. Erlebacher, *Adv. Mater.*, 16 (2004) 1897.
22. G. Madras and B. J. McCoy, *Chem. Eng. Sci.*, 59 (2004) 2753.
23. C. Y. Tai, J. F. Wu and R. W. Rousseau, *J. Cryst. Growth*, 116 (1992) 294.
24. M. S. Viola and G. D. Botsaris, *Chem. Eng. Sci.*, 34 (1979) 993.
25. V. Repain, G. Baudot, H. Ellmer and S. Rousset, *Mater. Sci. Eng. B*, 96 (2002) 178.
26. A. A. Schmidt, H. Eggers, K. Herwig and R. Anton, *Surf. Sci.*, 349 (1996) 301.
27. Y. Ding, A. Mathur, M. W. Chen and J. Erlebacher, *Angew. Chem., Int. Ed.*, 44 (2005) 4002.
28. S. Parida, D. Kramer, C. A. Volkert, H. R*ö*sner, J. Erlebacher and J. Weissm*ü*ller, *Phys. Rev. Lett.*, 97 (2006) 035504.
29. A. J. Forty and P. Durkin, *Philos. Mag. A*, 42 (1980) 295.
30. F. Jia, C. Yu, K. Deng and L. Zhang, *J. Phys. Chem. C*, 111 (2007) 8424.
31. J. Erlebacher, *J. Electrochem. Soc.*, 151 (2004) C614.
32. W. B. Liu, S. C. Zhang, N. Li, J. W. Zheng and Y. L. Xing, *J. Electrochem. Soc.*, 158 (2011) D91.
33. W. B. Liu, S. C. Zhang, N. Li, J. W. Zheng and Y. L. Xing, *Corrosion Sci.*, 53 (2011) 809.
34. Z. H. Zhang, Y. Wang, Y. Z. Wang, X. G. Wang, Z. Qi, H. Ji and C. C. Zhao, *Scr. Mater.*, 62 (2010) 137.
35. W. B. Liu, S. C. Zhang, N. Li, J. W. Zheng and Y. L. Xing, *J. Electrochem. Soc.*, 158 (2011) D611.
36. L. H. Qian and M. W. Chen, *Appl. Phys. Lett.*, 91 (2007) 083105.
37. G. Andreasen, M. Nazzarro, J. Ramirez, R. C. Salvarezza and A. J. Arvia, *J. Electrochem. Soc.*, 143 (1996) 466.
38. W. R. Tyson and W. A. Miller, *Surf. Sci.*, 62 (1977) 267.
39. S. C. Zhang, Y. L. Xing, W. B. Liu and J. W. Zheng, *The 15th International Meeting on Lithium Batteries, IMLB,* J. Electrochem. Soc., Abstract #82, Montréal, Canada, June 27-July 2, 2010.
40. J. W. Zheng, S. C. Zhang, W. B. Liu, Y. L. Xing and Z. J. Du, *J. New Mat. Electrochem. Systems*, 14 (2011) 213.
41. W. B. Liu, S. C. Zhang, J. W. Zheng and Y. L. Xing, *The 4th international conference on advanced lithium batteries for automobile application, ABAA-4,* Tianjin Institute of Power Sources & China Industrial Association of Power Sources, Abstract #108, Beijing, China, September 21-23, 2011.